HHS Public Access

Author manuscript

Epilepsy Res. Author manuscript; available in PMC 2020 December 08.

Published in final edited form as:

Epilepsy Res. ; 159: 106249. doi:10.1016/j.eplepsyres.2019.106249.

Rescue of PB-resistant neonatal seizures with single-dose of small-molecule TrkB antagonist show long-term benefits.

S.K. Kang[1], **S. Ammanuel**[2], **D.A. Adler**[2], **S.D. Kadam**[1,3]

[1]Department of Neuroscience, Hugo Moser Research Institute at Kennedy Krieger;

[2]Department of Biomedical Engineering, Johns Hopkins University, Baltimore, MD 21205, USA;

[3]Departments of Neurology, Johns Hopkins University School of Medicine, Baltimore, MD 21205

Abstract

A recently characterized CD-1 mouse model of phenobarbital (PB)-resistant neonatal ischemic-seizures (i.e.; unilateral carotid ligation) was shown to be associated with age-dependent (P7 vs. P10) acute seizure severity and PB-efficacy (i.e.; PB-resistant vs. PB-responsive). ANA12, a novel small-molecule TrkB antagonist, rescued the PB-resistance at P7 in a dose-dependent manner and prevented the post-ischemic downregulation of KCC2, the chief Cl- extruder in neurons. The long-term consequences of this novel rescue-intervention with ANA12+PB in P7 and P10 ligated pups was investigated and compared to the standard first-line protocol of PB-alone loading dose. The mice underwent neurobehavioral testing, 24h video-EEG-EMG monitoring and immunohistochemistry in ipsi- and contralateral cortices as adults, following the neonatal interventions. ANA12+PB rescued the emergence of hyperactivity in post-ischemic P7, but not in P10 pups as adults. ANA12+PB administration at neither P7 nor P10 significantly altered 24h macro-sleep architecture in adults when compared to PB-alone. Behavioral state-dependent gamma (35–50 Hz) power homeostasis showed the most significant between-group differences that were age-dependent. ANA12+PB treatment, but not PB-alone, rescued the loss of gamma power homeostasis present in P7 ligate-control but absent in P10 ligate group, highlighting the age-dependence. In contrast, PB-alone treatment, but not ANA-12+PB, significantly reduced the elevated delta-AUC observed in P10 ligate-controls, when PB is efficacious by itself. These results indicate that the rescue of acute PB-resistant neonatal seizures using a novel intervention positively modulates the long-term outcomes at P7 when the seizures are refractory.

Keywords

refractory seizures; hypoxic-ischemic encephalopathy; gamma oscillations; sleep dysfunction; hyperactivity

Corresponding Author: Shilpa D. Kadam, PhD, Neuroscience Laboratory, Hugo Moser Research Institute at Kennedy Krieger; Department of Neurology, Johns Hopkins University School of Medicine, 707 North Broadway, 400H; Baltimore, MD 21205, Phone: 443-923-2688, Fax: 443-923-2695, kadam@kennedykrieger.org.

Introduction

Hypoxic-ischemic encephalopathy (HIE) is a major underlying etiology of neonatal seizures, comprising 40% of new consults in the neonatal intensive care unit (Glass et al., 2010; Kang and Kadam, 2015; Mulkey and Swearingen, 2014). Neonatal seizures associated with HIE often display limited response to 1st-line anti-seizure medications (ASMs) like PB (Hellstrom-Westas et al., 2015; Painter et al., 1999), and result in significant long-term impairments of the central nervous system (Kharoshankaya et al., 2016; Murray et al., 2016; Pisani and Spagnoli, 2016). Even mild HIE is known to result in abnormal long-term outcomes (Conway et al., 2018). The extent to which acute symptomatic seizures contribute to the follow-on long-term co-morbidities remains unclear and difficult to parse clinically (Glass et al., 2011; Kwon et al., 2011), as the final outcomes are probably determined by multi-factorial interactions amongst the underlying etiology, seizure severity, genetic background, etc.

Preclinical models of acquired seizures have offered powerful insights into differential ASM efficacies as well as proteomic alterations during and after neonatal seizures, for which diverse etiology (i.e. chemo-convulsants, hypoxia, and ischemia) has been represented. However, limited progress has been made towards understanding the long-term consequences of acquired neonatal seizures (Kadam and Dudek, 2007; Rodriguez-Alvarez et al., 2015), and even more so for how ASMs affect the developing brain and thus the co-morbidities. For example, PB has clinically been shown to negatively impact long-term intellectual abilities (Camfield et al., 1979; Farwell et al., 1990). Early-life seizures (Jiang et al., 1998; Lynch et al., 2000; McCabe et al., 2001) and ASMs (Dean et al., 2002; Gedzelman and Meador, 2012; Kim et al., 2007) both exert adverse influence on brain development (Mayer et al., 2002). Therefore, how aggressively refractory neonatal-seizures should be treated has remained an active topic of debate, and has not been extensively investigated in animal models in long-term studies.

Here, the long-term neurophysiological outcomes of neonatal ischemic-seizures were assessed in a CD-1 mouse model that has been rigorously characterized to show age-dependent seizure severity (P7 vs. P10) and PB-efficacy (PB-alone vs. ANA12+PB) (Carter et al., 2018; Kang et al., 2015a; Kang et al., 2015b). For the same model our group has also previously reported age-dependent differential sleep dysfunction/qEEG biomarkers in untreated ischemic seizing pups (P7 vs. P10) when evaluated as adults (Kang et al., 2018). This finding was not unexpected, because abnormal sleep-wake cycling and background EEG are associated with unfavorable prognosis of HIE in neonates (Ahearne et al., 2016; Osredkar et al., 2005). Using behavioral tests, 24h v-qEEG (video-qEEG), and histology, this study evaluated the effects of two ASM therapies (standard PB-alone vs. novel ANA12+PB) administered at the two neonatal ages (P7 PB-resistant seizures vs. P10 PB-responsive seizures) of ischemic insult. Pairing acute neonatal seizure burdens and treatment responses with adult 24h v-qEEG recordings in the same individual mouse provides novel insights into how different treatment strategies for neonatal HIE-seizures can modulate long-term outcomes in adulthood. Evaluation of qEEG biomarkers can allow reliable and efficient detection of the underlying abnormal states of brain (i.e., neural co-morbidities) for which the behavioral manifestation may take place later in life. The translational value of qEEG

has been demonstrated by the increasing implementation of qEEG analyses in clinic (Claassen et al., 2016; Heinrich et al., 2014) and in pre-clinical studies (Kent et al., 2019; Zanettini et al., 2018) in diverse contexts. The data indicate that refractory neonatal seizures have significant long-term outcomes and reversing early refractoriness can help alleviate these outcomes.

Materials and Methods

1. Experimental design

Four experimental groups were studied: 1) P7 PB-alone, 2) P7 ANA12+PB, 3) P10 PB-alone, and 4) P10 ANA12+PB: total n=34 mice. Whenever necessary, data from these groups were also compared to similar data from three other groups (sham, P7 ligate, and P10 ligate; total n=41 mice) that was published previously as a pilot study (Kang et al., 2018). The experiments and data for all seven groups were acquired simultaneously. On day of ligation surgery (P7 or P10), pups were randomly assigned (n=8–12 each of the four groups) and toe-clipped under anesthesia for future identification. Briefly, following induction of acute symptomatic seizures with ischemia at either P7 or P10 and subsequent acquisition of acute EEG for seizure analyses, mice were allowed to mature into adulthood followed by same-sex housing. A battery of behavioral tests was conducted around week 12–13, followed by head-mount implantation surgery (described below). At week 15, mice underwent 24h-video EEG recording for sleep structure and qEEG analyses. Lastly, a set of standard behavioral tests were conducted at week 16, followed by brain harvests and histology around week 18. Experimental schematics are described in Figure 1A. Experimenters remained blinded to the treatment groups for data analyses.

2. Mice

CD-1 mice were purchased from Charles River Laboratories Inc. (Wilmington, MA, USA), and litters of pups arrived on postnatal day 3 (P3). Mice were housed in polycarbonate cages on a 12h Light/Dark cycle with *ad libitum* access to food and water. All studies were approved by the Committee on the Ethics of Animal Experiments of the Johns Hopkins University, and adhered to the recommendations in the Guide for Care and Use of Laboratory Animals of the National Institutes of Health. After ligation surgery, mice were weaned at P21 and group-housed 4–5 same-sex mice per cage until head mount surgery at week 14, after which the mice were single-housed until the end of study.

2.1 Ligation surgery, acute video-EEG recording, and seizure burdens—

Permanent double-ligation of right common carotid artery was utilized to induce neonatal ischemia in pups anesthetized with 4–1.5% isoflurane as previously described; sham controls underwent a mock-surgery except for the ligation. This unilateral ligation in the neonatal model done without the transection of the carotid artery results in ischemia-induced transient seizures in CD-1 pups without the occurrence of stroke related infarct injury when evaluated at P18 (Kang et al., 2015b). For drug injections, ANA12 (2.5mg/kg) was administered immediately after ligation surgery, and PB (25mg/kg) was delivered at 1h post-ligation. Additional information on the types and anatomical locations of EEG electrodes can be found in our previous publication (Kang et al., 2018). Two hours of continuous acute

EEG data were acquired and analyzed using Sirenia Acquisition/Seizure software (Pinnacle Technologies; Lawrence, KS); seizures were defined as epileptiform discharges lasting >6s (Kang et al., 2015b). For PB efficacy (Fig. 1B), the following calculation has been used: PB efficacy = $100 \times [1 - (TSB_{Post\ PB}/TSB_{Pre\ PB})]$; TSB = Total Seizure Burden.

3. Neurobehavioral tests

At postnatal week 12–13, mice were tested for open-field, Y-maze, elevated plus maze, social interaction, and pre-pulse inhibition in order. All procedures were conducted with minimal handling under strict supervision of the Behavior Core at the Brain Science Institute, Johns Hopkins University and were performed exactly the same way as they were described previously (Kang et al., 2018). Additional tests for open-field and social interaction were conducted at postnatal week 17; same as described previously for pilot study (Kang et al., 2018). Prior to open-field testing, daily habituation of mice (5 min duration) was done, and each test was conducted during daytime, separated by approximately 48h. Additional details are available in our previous publication (Kang et al., 2018). Below are brief descriptions of how the tests were conducted.

3.1 Open-Field (OF) Test and hyperactive mice identification.—Mice were placed in a square PAS- Open field station (16”W × 16”D × 15H; San Diego Instruments, CA) at the center, allowed to explore freely for 25 min. Data was acquired through PAS software using invisible infrared light beams (16 × 16) set on the four sides of the walls. Activity levels were quantitated per 5 min bin, and each mouse underwent OF session twice: once at PND 80 and again at PND 130. Based on statistical detection of outliers, hyperactive mice were defined as the animals which met Rosner’s Extreme Studentized Deviate test for multiple outliers (two-sided test, significance level set at 0.00001).

3.2 Y-maze—Spatial memory function was tested using two sessions of Y-maze. On day of 1st Y-maze, mice were allowed to explore each arm of Y-maze starting at an arm, while the sequence in which it navigated each arm was recorded and analyzed. On day of 2nd Y-maze, one arm was blocked with a transparent barrier, while mice were allowed to explore the apparatus for 5 min. After 20 min, the barrier was removed, and mice were allowed to explore freely, to see whether it would prefer the novel arm that it was not allowed to explore during the exploratory session. Data were analyzed as follows; for YM1, percent score = [(# of Alternations/Total # of trials) *100]: for YM2, percent score = 100*(time spent in novel arm/total test duration).

3.3 Elevated Plus Maze—Spatial anxiety levels were assessed using Elevated plus maze (EPM) on a plus-sign shape apparatus with crossing of an open arm and a closed arm at an elevation of 2 feet. The time spent in the open arms and closed arms were manually scored by an observer blind to experimental groups. For analyses: % score = 100*(time spent in open arm/total test duration).

3.4 Pre-pulse Inhibition (PPI)—Startle reflex measurement system (Ohara Ika Sangyo, Tokyo, Japan) was utilized to measure pre-pulse-inhibition. After being placed in a Plexiglas cylindrical tube with limited space adjustment capability, each mouse was habituated for 5

min with 70dB background noise. Each testing session began with presentations of a 120dB (100ms, broadband burst) pulse repeated 10 times with 20s intervals, followed by a series of randomized presentations of pre-pulses (20ms broadband burst) of levels (74–120), (78–120), (82–120), (86–120), (90–120), 80ms prior to the 120 pulse. Five blocks of the six trial types were presented in a pseudorandom order, while each trial type was presented at least once within a block, and the startle response was measured. % PPI was calculated as follows: [100*(amplitude at 120dB - amplitude at X prepulse dB)/amplitude at 120dB]

3.5 Social Interaction (SI)—Three chamber paradigm (Billingslea, 2007) was utilized to measure social abilities at PND 80 and PND130. In a Plexiglas apparatus ($30\times36\times17cm^3$), each mouse was habituated for 5 mins 2 days prior to the day of test, which consist of two parts that were 30 min apart: 1) social recognition, 2) social preference. Each mouse started at the center (“start”) chamber (15×10 cm; Habitest Runway; Coulbourn Instruments) separated from the other (left and right) chambers by drop doors. Placed in the left and right chambers were small conical cages with an alien conspecific adult mouse in each, and access to the alien mouse was limited by a grid with 1-cm holes. This paradigm and protocol has been previously described (Nadler et al., 2004): for data analyses, the SI index was calculated as novel chamber exploration time/(total exploration time – time spent in the middle starting chamber) during the test phase.

4. Head mount surgery for EEG in adult mice and quantitative EEG (qEEG) analysis

As adults at postnatal week 14, mice underwent surgery for implantation of EEG/EMG recording electrodes. Number of mice allocated for each group is described in Supplementary table 2. The surgery protocol and anatomical location of electrode coordinates for EEG and EMG electrodes were the same as reported for the pilot study for long-term outcomes in untreated neonatal ischemic pups (Kang et al., 2018). Following 4–6 recovery days, 24h continuous vEEG/EMG was recorded in a recording chamber with a tethered pre-amplifier/commutator under a top-view infrared camera. All EEG data were scored manually as 10s epochs of recording periods into three behavioral states; 1.wake and 2.NREM sleep and 3. REM sleep, using video, EEG and EMG as a guide. The entirety of EEG data was reviewed manually by a scorer blind to treatment group. Possible artifacts (i.e. scratching, chewing, etc) were identified and excluded from analysis.

Spectral power analysis was performed on the recorded EEGs (Frequency bands: Delta 0.5–4 Hz, Theta 5.5–8.5 Hz, Alpha 8–13 Hz, Beta 13–30 Hz and Gamma 35–50 Hz). Raw EEG traces underwent fast-Fourier transformation (FFT) using data analysis modules in Sirenia Sleep (Pinnacle Tech Inc., Kansas USA). Spectral power was calculated for every scored 10 sec epoch for the 24h EEG recording and exported into excel using the sleep score module (Sirenia, Pinnacle Technologies Inc. Kansas, USA), similar to previous protocols (Johnston et al., 2014; Kang et al., 2018). EEG artifacts identified during manual scoring for behavioral states (sleep/wake) were left unscored so that there was no contamination of qEEG data for spectral power analysis. Total Delta power for each consecutive wake and sleep cycle, was calculated using the area under the curve (AUC) analysis. AUC was calculated with trapezoidal summations by calculating the area under each sleep or wake cycle. Delta power for every sequential 10 sec epoch within that cycle was calculated as a

trapezoid using R statistical software. Total Gamma AUC and wake Gamma AUC was similarly analyzed. Sleep Gamma fell gradually over the duration of every sleep cycle; therefore the total 24h sleep AUC was calculated as:

Sleep gamma AUC 24h = Total gamma AUC 24h – Total wake gamma AUC 24h.

Behavioral-state dependent gamma homeostasis was calculated for two independent transition states for each mouse (i.e.; falling asleep and waking up). The slope of the spectral power change for gamma during behavioral transitions from wake to sleep states was calculated as means over a period of 10 minutes from the initiation of each sleep cycle and the last 10 minutes of its preceding wake-cycle. The reverse was applied to the sleep-wake transitions. The rate of rise or fall of gamma for each behavioral transition state was then calculated as slope between these mean values. The theta-beta ratio (TBR) was calculated by dividing theta power at each 10 sec epoch of EEG by its corresponding beta power: TBR = Theta power/beta power; similar to published protocols (Kang et al., 2018).

5. Immunohistochemical analyses

All adult mice following chronic 24h EEG underwent transcardiac perfusions (ice-cold PBS followed by 10% formalin) after being anesthetized with chloral hydrate (90 mg/ml; IP). Brains were post-fixed in 10% formalin overnight and cryoprotected sequentially in 15% and 30% sucrose in PBS at 4°C. Cryoprotected brains were flash frozen on dry ice and stored at −80 °C. Brains were sectioned at 14μm as serial sections on a cryostat, mounted on superfrost slides and stored at −30°C. Sections underwent heat antigen retrieval in pH 6 sodium citrate buffer at 97°C for 40 minutes. With evidence of spontaneous chronic generalized seizures in adult mice with history of refractory neonatal seizures at P7 in this CD-1 mouse model (Kang et al., 2018), markers of inhibition in the somatosensory cortex to compare the ipsi- vs. contralateral hemisphere (ischemic vs. non-ischemic) were investigated. The somatosensory cortex was chosen because with the common carotid artery ligation used in this study, the maximum drop in perfusion pressure is known to occur in the perfusion territory of the middle cerebral artery territory (Kadam and Dudek, 2007). This results in significant epileptogenesis in the ipsilateral ischemic cortex (Kadam and Dudek, 2016) in the somatosensory cortex and in the long-term is associated with spontaneous recurrent seizures (Kadam et al., 2010b). Sections were blocked in 5% normal serum before overnight incubation with primary antibodies in 3% in PBS-T [vGAT (1:1000) Synaptic Systems, 131 011; GAD67 (1:1000), Chemicon International, MAB5406; Gephyrin (1:500) AB32206 Abcam]. Sections were washed in PBS and incubated with secondary antibodies for 2h at room temperature. All sections were counterstained with nuclear stain Hoechst (1:2000, Invitrogen). After cover-slipping, slides were imaged as Z stacks using a Zeiss apotome. All 40X images of the cortical layers 2–3 and 5–6 of the ipsi- and contralateral somatosensory cortices were taken from 20um thick coronal sections at Bregma −1.2 to −1.7 (Franklin and Paxinos mouse atlas). All Z-stack images were analyzed with Axiovision software. The contrast and brightness of all images were adjusted similarly. The total counts of puncta were quantified using ImageJ (NIH, USA) under high magnification (40X). Similar to previous protocols (Kang et al., 2014), investigators blinded to experimental groups manually counted somatic and perisomatic puncta for four randomly selected

neurons per 150×150 pixel ROI frame exported using data analysis modules in AxioVision 64.

Statistical analyses

Statistical analyses were conducted using Excel 2010 (Microsoft), SPSS21 (IBM), or Prism7 (GraphPad). Group means were compared using One-way ANOVA, and the p-values were reported along with F statistic reported as F (df_{time}, df_{error}). Appropriate post-hoc comparisons (Bonferroni or Tukey's) were followed when needed. Paired t-tests and two-way ANOVA were used when appropriate (i.e. within-group comparison by cycles). The alpha value was set at 0.05 to be considered statistically significant. Outliers were excluded by Rosner's Extreme Studentized Deviate test for multiple outliers and the resultant distribution normality was justified by Shapiro-Wilks test, a goodness-of-the-fit test. For violin plots shown in Figure 5A–B, statistical outliers were excluded by robust regression and outlier removal (ROUT) method at 5% threshold in GraphPad Prism. All data are reported as mean ± S.E.M.

Results

Age-dependent seizure severity and PB-efficacy

In addition to the neonatal ischemic insult at P7 and P10 to induce ischemic neonatal seizures, a subset of mouse pups (see Supplementary Table 1) underwent 2h of continuous EEG recording of the acute ischemic seizures. It was done to help verify the previously characterized seizure burden profiles and response to anti-seizure medications (ASMs) for the model (Figure 1B and C). This acute EEG quantitation also set the acute baseline for the follow-on 24h recordings in the same pups as adults. Acute seizure burden for the 1st baseline hour (pre-PB) was compared to the 2nd hour (post-PB), and the PB-efficacy was calculated as percent seizure burden reduction during the 2nd hour in comparison to the 1st baseline hour (Figure 1B). Neonatal ischemic-seizures showed age-dependent severity and PB-responsiveness, the latter of which was improved by ANA12, a small-molecule TrkB antagonist (Kang et al., 2015a; Kang et al., 2015b). PB was significantly more efficacious in P10 compared to P7 mice (PB-resistant; ♦ P7 vs. P10), and ANA12 significantly reversed PB non-efficacy in the P7 ligate group (Figure 1B ♦ vs. ♦ P7; p=0.0002 and p=0.0017 respectively; One-way ANOVA, $F_{3,26}$=15.15, Bonferroni's multiple comparisons test). Representative EEG traces for ANA12+PB treated groups for P7 and P10 illustrate PB efficacy pre- vs. post-PB injection, especially for P10 (Figure 1C). The non-efficacy of PB-alone treatment at P7 established the acute PB-refractoriness for this study (Kang et al., 2015b). The P10 seizures were significantly PB-responsive, establishing the age-dependent differential for PB-efficacy for the same ischemic insult in the model for neonatal seizures. Summary of acute EEG seizures by total seizure burden and ictal events is compiled in Supplementary Table 1.

No emergence of hyperactivity in P7 ANA12+PB group of mice

Neonatal pups with untreated ischemic-seizures were previously shown to develop behavioral deficits in adulthood such as hyperactivity and delayed spatial habituation in

open-field (OF) testing (Kang et al., 2018). In this study, neither P7 nor P10 treated groups showed significant difference in their total activity levels: (Figure 2A; p=0.3 $F_{5,49}$=1.25 p=0.4 $F_{5,44}$=0.99 One-way ANOVA; Tukey's, for P80 and P130 in order) compared to untreated ligate-controls (Fig 2A, dotted line). The average total activity in the P10 ANA12+PB group was significantly higher compared to sham-controls (Fig 2A; solid line) at P80 (p=0.02, $F_{6,68}$=2.1 One-way ANOVA Tukey's) but not significant at P130 (p= 0.98, $F_{6,62}$=1.68). At P80, P7 groups, both PB-treated and ANA12+PB treated, but not P10 groups, achieved spatial habituation by the end of the testing (Figure 2B top &C left panels; p<0.05 compared to the activity levels during the 1st interval; @: p=0.034 #: p=0.043 repeated measures ANOVA). In contrast, at P130, only the P7 ANA12+PB and P10 PB-alone group achieved spatial habituation (Figure 2B bottom panels & C right panels; #: p=0.004, @: p=0.043). Similar to what was reported in mice with a history of neonatal ischemic-seizures for the model, a subset of mice developed hyperactivity in open-field (OF; n=1 mouse from P7 PB and 3 mice from P10 ANA12 PB); hyperactivity threshold was defined as previously set (i.e. 6,000 beam break counts in either P80 or P130 OF testing). Exclusion of hyperactive mice did not restore the group mean habituation in either P7 PB or P10 ANA12+PB group (data not shown).

Behavioral tests for cognitive and social abilities.

An additional battery of neurobehavioral tests were conducted to screen for cognitive and social deficits in the mice treated with PB and ANA12+PB at P80 or P130. Previously reported behavioral test outcomes for the mouse model showed that un-treated ligated mice did not exhibit significant deficits in their neurobehavioral abilities due to large variability (Kang et al., 2018). Similarly in this study, the ANA12+PB and the PB-alone treatments did not result in significant behavioral deficits on the tests as adults (open-field, Y-maze, elevated plus maze, pre-pulse inhibition, and social interaction; summarized in Supplementary figure 1). In summary, standard behavioral testing alone was not a reliable biomarker of the long-term effects of refractory neonatal seizures in this model due to emergence of hyperactivity in a sub-set of mice in OF and variability in the other behavioral tests.

Altered hypnograms in ligate-treated groups by age

The pilot study investigating the role of neonatal age on the long-term outcomes of untreated ischemic seizures in the same CD-1 strain identified several markers of sleep dysfunction on their hypnograms generated through analysis of 24h continuous EEG recordings. These included the loss of diurnal variation in NREM/REM cycle durations and the emergence of significantly long-wake-cycles (Kang et al., 2018).

At P10, in this study, PB-alone significantly reversed the duration of the longest wakes detected in their age-matched ligate-controls in the pilot study, thus making them similar to naïve controls (Figure 3C; p<0.05 $F_{5,54}$=2.38 One-way ANOVA). NREM diurnal variation (NREM duration in light vs. dark cycle), previously lost in the P7 ligate-controls, was restored in PB-alone group but not in ANA12+PB group (Figure 3D blue; p<0.05 paired t test, p=0.053 $F_{2,64}$=1.20 two-way ANOVA): interaction p=0.39 and 0.61 for P7 and P10 respectively. The P7 PB-alone group had longer NREM sleeps during the light cycle. For the

P10 group, the NREM diurnal variation, present in P10 ligate-controls, was now lost both in the PB-alone and ANA12+PB treated groups. Diurnal variation in REM, absent in P7 and P10 ligate-controls, remained absent in all treatment groups (Figure 3D red).

Delta power during slow-wave-sleep (SWS)

Significant alterations in delta-wave amplitude and SWS (NREM) were previously observed for the ligate-control mice in the pilot study (Kang et al., 2018). Briefly, significantly higher delta-AUC was detected in P10 ligate-controls during sleep cycles, potentially as a compensation mechanism for the emergence of the significantly long wake-cycles. This however was not detected in P7 ligate-controls with similar emergence of long-wake-cycles indicating a failure of compensation for slow-wave-sleep in the P7 untreated group. In this study, similar trends were detected (Figure 4; lines for age-matched ligate-control means from pilot report). For P7 treatment groups, delta-wave AUCs, split by wake vs. sleep (NREM), were not significantly different from P7 ligate-controls (Figure 4). P10 PB-alone group, but not P10 ANA12+PB, showed a significant reduction in the delta-AUC during both wake and sleep during light cycle ($p<0.05$ and $p<0.01$ in order; One-way ANOVA $F_{3,38}=3.0$ and $F_{3,38}=6.6$) and only wake during dark cycle ($p<0.01$; One-way ANOVA, $F_{3,38}=6.3$). Numbers of wake/sleep cycles were similar across the different treatment groups.

Gamma power as a function of behavioral-state

Gamma frequency oscillations are strongly associated with wakefulness and attention. Gamma slopes during transitions from sleep to wake-states and vice-versa (i.e. rate of rise of gamma power: sleep to wake, rate of fall of gamma power: wake to sleep) were analyzed (Fig 5A and B). For this analysis, gamma power data from the age-matched untreated ligate-controls (Kang et al., 2018) were included in this analysis for comparison. The sham-group exhibited significantly differential regulation of gamma power slopes during behavioral transitions (i.e.; rise vs. fall in gamma power, Repeated measures ANOVA, $F_{7,1293}=6.76$, $P<0.0001$). In contrast, P7 ligate-control and ligate+PB failed to show significant changes in gamma power homeostasis associated with the same behavioral state transitions ($P=0.68$, 0.48 respectively). All P10 treatment groups exhibited behavioral state-dependent modulation of gamma power slopes similar to the sham-controls (Repeated measures ANOVA $F_{7,1429}=13.22$). Gamma power increased during wake-states and exploration and decreased during NREM sleep in sham-controls (Fig 5C). In contrast, the P7 PB-alone group had significantly higher gamma power during sleep compared to both sham-controls and P7 ligate-controls (One-way ANOVA $F_{6,62}=3.0$ $p=0.011$; $p=0.041$ vs. sham, $p=0.041$ vs. P7 ligate-control respectively; Figure 5D and E). Acute ANA12+PB novel intervention at P7 significantly rescued the emergence of the abnormally high sleep gamma back to sham levels in the same pups as adults ($p>0.9999$ vs. sham, Fig. 5F).

Gamma power fell gradually during wake to sleep (WTS) transitions and rose abruptly during sleep to wake (STW) transitions (see Fig. 5C). Therefore, in sham-controls, gamma slopes were significantly different between the two independent WTS and STW transition states (t-test assuming unequal variance; $t_{312}<0.0001$; Figure 5C & G). At P7, this difference was lost in ligate-control mice that was not rescued by PB (Ligate-control: t312=0.363; Ligate+PB: t224=0.182; Figure 5D–E, H). Acute ANA12+PB intervention at P7

significantly rescued and restored the difference in gamma power transitions between WTS and STW (t_{222}=0.0086; Figure 5F–H) in the same pups as adults. In summary, at P7, PB-refractory seizures lead to the loss of behavioral-state homeostasis of gamma oscillations. ANA12+PB intervention at neonatal age of P7, rescued this behavioral-state homeostasis of gamma power oscillations during in the same pups as adults indicating long-term benefit of a single-dose intervention with ANA-12.

At P10, when the seizures are PB-responsive (Supplementary table 1), both the WTS and STW gamma slopes retained their behavioral-state homeostasis in the same pups as adults and remained significantly different from each other (Ligate: t_{272}<0.0001; Ligate+PB: t_{340}<0.0001; Ligate+ANA12+PB: t_{206}=0.0002; Figure 5I). Therefore gamma power homeostasis was significantly impaired following P7 PB-resistant seizures but not the PB-responsive P10 seizures, highlighting the age-dependent differential long-term outcomes for the same insult.

Beta/Theta power AUC

Behavioral-state modulation of beta and theta power AUCs were not significantly different for either treatment group at P7 compared to age-matched ligate-controls. At P10, comparisons of wake and NREM sleep related beta AUC, revealed that the significant increase in beta power AUC in P10 ligate-controls during both wake and NREM sleep was significantly reduced in P10 PB-alone group (Supplementary figure 2; p=0.027 and 0.015 during sleep and wake; One-way ANOVA, $F_{6,63}$=3.0and $F_{6,63}$=3.1; Bonferroni post-hoc). In contrast, P10 ANA12+PB group lost the significance in reduction of beta AUC detected in the PB-alone treatment (p=1.0 vs. P10 ligate control for both wake and sleep). No other between-group comparisons for the different treatment groups were statistically significant. Theta power AUC revealed a similar finding that the P10 PB-alone group, but not for the P10 ANA12+PB group, exhibited a significantly lower theta power AUC, both during wake and sleep compared to P10 ligate-controls (Supplementary figure 2; p=0.002 and 0.003 during sleep and wake respectively; One-way ANOVA, $F_{6,62}$=5.0 and $F_{6,63}$=4.2; Bonferroni post-hoc). Overall, the reductions in the beta/theta AUCs observed were specific to P10 PB-alone mice.

Markers of GABAergic synapses

Cortical gamma oscillations are driven by interneuron activity. To look at inhibitory synapses, IHC-protocols labeled gephyrin, GAD67 and vGAT. The somatosensory cortex was chosen as it is perfused by the middle-cerebral artery and therefore at the center of the drop in perfusion pressure associated with the P7 and P10 ligation of the common carotid artery due to lack of collateral circulation from the branches of the contralateral carotid (Kadam and Dudek, 2007). Puncta for each protein were quantified to evaluate expression of pre- and post-synaptic proteins at inhibitory synapses, specifically in layer 2–3 and 5–6 of somatosensory cortex [see Supplementary Table 4 for data for left (contralateral control) and right (ipsilateral to ischemia) cortical hemispheres].

Between P7 groups, layer 2/3 counts were significantly different (p=0.048, One-way-ANOVA); post-hoc comparisons however showed no significance between ligate-controls

and ANA12+PB (p=0.065). For layer 5/6 group, the differences were significant (ANOVA p=.044, Post-hoc naïve control vs. ANA12+PB; p=0.044). Within groups, P7 ligate-controls showed an inter-hemispheric difference in the expression levels of vGAT puncta (Image J) in Layer 5–6; which were significantly lower in the contralateral-cortex (p=0.035, n=7; paired t-test). This hemispheric difference was due to somatic rather than perisomatic counts of vGAT puncta (p=0.035 vs. p=0.17 respectively; n=7; paired t-test; Figure 6). This interhemispheric difference was absent in P7 PB (p=0.57, n=2) and P7 ANA12+PB group (p=0.77, n=4). However, layer 2/3 showed a significant interhemispheric difference in vGAT puncta only in the P7 ANA12+PB group. This was associated with similar interhemispheric difference in the GAD67 puncta for the same group ($p<0.05$). P10 ligate-controls also showed a significant downregulation of vGAT and GAD67 in layer 5–6 and 2–3 respectively, ipsilateral compared to contralateral cortex (See Suppl. Table 4; p=0.010, n=5; and p=0.022, n=6 respectively, paired t-test). This difference was absent in both the P10 PB and ANA12+PB groups (p=0.89 and p=0.22 respectively; paired t-test). No group differences were detected for gephyrin puncta (Suppl. Fig. 3).

Discussion

An important question in the neonatal seizure field has been, how aggressively to treat acute symptomatic neonatal seizures? Especially those that are refractory to first-line ASMs? (Abend and Wusthoff, 2012; Chapman et al., 2012; Jobe, 2009). PB is the preferred first-line ASM used for HIE seizures (Boylan, 2002) and mean clinical loading doses for PB are ~20 mg/kg for neonates (Glass et al., 2019). Loading doses of PB are often followed by repeat dosing when the first dose fails, going to a high of 60–80mg/kg drug load within a 24h period (Ajayi et al., 1998; Donn et al., 1985). However, PB can have both acute and long-term detrimental side-effects without any additional beneficial acute seizure suppression efficacy (Bittigau et al., 2003; Markowitz et al., 2011), and refractory seizures themselves can have long-term effects on brain development (Bjorkman et al., 2010; Jobe, 2009; Kang et al., 2018; Kang and Kadam, 2015). We have previously shown that neonatal seizures have age-dependent long-term effects on sleep dysfunction (Kang et al., 2018). This study explored the effects of standard and novel adjunct ASM interventions in modulating such long-term co-morbidities. The results of this study showed that PB-alone given to P7 seizing neonates, in which seizures are known to be refractory to PB, either failed to improve or exerted deleterious effects on the long-term outcomes in the same mice, as adults. In contrast, ANA12+PB not only rescued the PB-resistant seizures acutely at P7 but also alleviated emergence of hyperactivity and abnormally long wake-cycles at P130 and most importantly, corrected the loss of behavioral-state homeostatic modulation of gamma oscillations. Therefore, any aggressive management of neonatal seizures needs to be evidence based, both acutely to document the efficacy and long-term to evaluate effect on identifiable biomarkers underlying co-morbidities. This study identifies the qEEG biomarkers underlying the long-term effects of refractory neonatal seizures and their amenability to reversal when the acute refractory seizures are rescued.

Similar beneficial effects of ANA12+PB (i.e. delta AUC reversal in Figure 4) were not evident in the treated group of P10 mice, the age at which the seizures are already PB-responsive and would not need an additional intervention like ANA12. We have recently

shown that the excitotoxicity related activation of the TrkB-PLC$^{\gamma}$ pathway is age-specific in this model and particularly at P7 when the seizures are PB-resistant (Carter et al., 2018). This study showed that the long-term effects of the acute ANA12-mediated TrkB antagonisation and resulting reversal of PB-resistance at neonatal ages P7 vs. P10 were also age-specific (Figure 1B). The P10, PB-alone group of adult mice with PB-responsive seizures did better than their ANA12+PB treated counter-parts as adults, indicating that PB-resistance may be dependent on the age-specific BDNF-TrkB interactions during the neonatal period. This may likely explain the ANA12-mediated long-term beneficial results reported here for P7-treated pups vs. not for P10-treated pups.

ANA12+PB rescued PB-resistance at P7; did not improve PB-efficacy at P10

Analyses of acute EEGs run on a sub-set of the treated pups allowed confirmation that ANA12 was able to rescue PB-resistance at P7 for this long-term study before the mice matured into adulthood. At P10 when the ischemic seizures are known to be responsive to the same dose of PB, ANA12+PB did not further improve PB-efficacy significantly. Acutely, during the time-point of the neonatal seizures, the role of the TrkB receptor pathway activation following ischemia in the emergence of refractory seizures in the model was found to be age-dependent (Carter et al., 2018). Differential PB-efficacy on electrographic seizures by single-dose ANA12 at P7 vs. P10 established the paradigm for evaluating the long-term behavioral outcomes and qEEG markers for the same pups with and without neonatally rescued refractoriness.

No hyperactivity/seizures detected in post-ischemic P7 mice treated with ANA12+PB

We have previously shown the emergence of hyperactivity in a sub-set of adult mice with the history of neonatal ischemia both at P7 and P10 (Kang et al., 2018). Post-ischemic progressive hyperactivity was also previously documented in the same strain with P12 ischemic insults that was not detectable just 1 month after the insult (Kadam and Dudek, 2007; Kadam et al., 2010a). In this study, no hyperactive mice were identified in the ANA12+PB group at 4 months of age in the P7 group. In contrast, hyperactive mice were identified in the ANA12+PB group of mice in the P10 group. Altered spatial habituation among treatment groups suggests impaired primal learning and memory, which also have been implicated in experimental models of ADHD (Zhuang et al., 2001), AD (Bales et al., 2006), and stroke (Kadam et al., 2010a). No spontaneous seizures were recorded in the ANA12+PB treated groups of mice at either age within the 24h recording period. In contrast, one spontaneous seizure was recorded in a P7 ligate, and another P7 ligate PB-only mouse showed multiple seizures that were fatal. Clinically, epilepsy is strongly associated with ADHD and hyperactivity (Williams et al., 2016). Long-term effects of neonatal ischemia and seizures may play a role in the altered maturation of the inhibitory system that results in the epilepsy and associated hyperactivity.

Significantly prolonged wake-cycle dysfunction in ligate-group repressed by PB and not changed by ANA12+PB at P7.

Neonatal ischemic insults resulted in significantly long wake-cycles in untreated seizing mice when evaluated as 4 month old adults (Kang et al., 2018), both in the P7 and P10 group of ligate-control. The treated pups in this study did not exhibit similar long wake-cycles in

the P7 or P10 groups, both with the PB-only and ANA12+PB treatments. Previous work also showed that ligate-controls exhibited loss of diurnal variation in NREM and REM compared to sham: figure 3D–E in (Kang et al., 2018). PB-alone treatment restored the NREM diurnal variation (light vs. dark) only in P7 group not in P10. This phenotypic rescue was no longer present in ANA-12+PB group; despite the higher seizure suppression was achieved in P7 ANA12+PB group. This indicates that the restoration of NREM diurnal variation may be independent of the degree of seizure-control. In contrast, the significant reduction in the duration of longest wake only in P10 group but not in P7 suggests that antagonism of TrkB signaling may have a role modulating duration of the wake state.

PB-induced reduction of Delta-AUC previously elevated in P10 ligate-control

Delta wave (0.5–4Hz) amplitude as well as AUC represents sleep quality and/or pressure during slow-wave-sleep (SWS-NREM). Our previous study indicated a potential age-dependent SWS compensation for the long-wakes, such that the long-wake cycles present in P10 ligate-control lead to higher delta-amplitude during NREM, likely due to the increased sleep pressure. In this study, PB-alone treatment, but not ANA-12+PB, significantly reduced the elevated delta-AUC observed in P10 ligate-controls. This may be explained by the significant reduction of longest wake cycle duration observed only in the P10 PB-alone group (Figure 3C).

ANA12+PB rescued the behavioral state-dependent homeostasis for gamma frequency activity at P7 but not at P10

Balance of cortical excitatory and inhibitory circuits driven by interneurons is known to underlie the generation of gamma oscillations (Buzsaki and Wang, 2012; Rubenstein, 2010). EEG gamma frequency oscillations occur in a behavioral state-dependent manner and are critical for the neural synchronization in active wake-cycles and during REM sleep (Hwang et al., 2013; Maloney et al., 1997). Increased gamma power and neural activity synchronization is generally observed during explorative activity and cognitive tasks (Cantero et al., 2004; Nowak et al., 2018), and gamma oscillation has recently been demonstrated to provide reliable diagnosis of autism spectrum disorder, serving as a clinical biomarker (An et al., 2018). In this study, we evaluated the behavioral state-dependent modulation of gamma power during transitions from wake to sleep and sleep to wake. Overall gamma power (AUC) was higher during wakefulness and lower during sleep (Gross and Gotman, 1999). The rate-of-fall or rise of gamma during wake-sleep transitions helped investigate the density of gamma oscillations during different behavioral states that are known to reflect rhythmic firing of inhibitory interneurons, entraining neuronal firing (Buzsaki and Wang, 2012).

At P7, both the ligate group and PB-only treated group showed severe impairment in the behavioral-state modulation of gamma power. ANA12+PB rescued the ischemia induced loss of gamma oscillation homeostasis associated with sleep-wake state transitions that the standard PB-alone treatment failed to rescue at P7. Interestingly, P10 neonatal ischemia did not lead to a similar dysfunction of gamma oscillation modulation during behavioral-state transitions further highlighting the role of age at ischemia and PB-refractoriness of neonatal seizures in the long-term outcomes in the same mice as adults.

Immunohistological analyses of GABAergic synapse markers

Neonatal ischemia, refractory seizures, and ASM treatments can cause long-term and permanent alterations in brain proteome. We have previously recorded and reported spontaneous seizure occurrence in adult CD-1 mice with a history of P7 refractory ischemic seizures (Kang et al., 2018). Investigation of inter-hemispheric and treatment-group specific changes in the expression levels of GABAergic synaptic markers (Figure 6; Supplementary Figure 3, and Table 4) could underlie the qEEG findings demonstrating differential phenotypes of seizure-refractoriness and PB-efficacy at P7 vs. P10. We found significant reduction in counts of vGAT somatic puncta in layer 5/6 of the ipsilateral somatosensory cortex in P7 but not P10 group of ligates. Downregulation of vGAT following ischemic insults or excitotoxicity has been previously documented in adult brain. Dysregulation of presynaptic element (i.e. vGAT or GAD67) could contribute to the emergence of follow-on epilepsy in the model, and thus warrants further evaluation. More importantly the specific deficit in peri-somatic vGAT could indicate dysfunction in the neuronal innervation by inhibitory fast-spiking parvalbumin interneurons that are known to drive cortical-gamma oscillations (Sohal et al., 2009). Based on the pilot results reported here, future studies should pursue long-term transcriptomic or proteomic changes in this mouse model of refractory neonatal seizures to ascertain mechanism underlying epileptogenesis and cortical dysfunction.

Single-dose acute intervention with ANA12 has long-term benefits in adult mice

Acute dosing with ANA12+PB rescued the neonatal ischemic refractory seizures at P7. We have shown that this rescue is associated with rescue of post-ischemic KCC2 down-regulation. The long-term beneficial effects reported in this study show that transient downregulation of KCC2 in models of HIE can be critical in the severity of the long-term comorbidities associated with behavioral and learning impairments. KCC2 is heavily expressed in interneurons and is critical to their migration and cortical innervation (Bortone and Polleux, 2009). Early deficits in these cues due to downregulation of KCC2 by ischemic insults and severe refractory neonatal seizures may be mechanisms by which the resulting E/I imbalance leads to long-term co-morbidities and follow-on epilepsy.

Conclusions

The TrkB pathway seems to play a significant role not only in the emergence of refractory neonatal seizures (Carter et al., 2018) but also in the long-term co-morbidities associated with them (Kang et al., 2018). This study investigated the long-term effects of a novel small-molecule TrkB antagonist on these long-term outcomes when used as an intervention to rescue PB-resistance as neonates. The results found that rescuing PB-resistance in neonates not only significantly reduced the acute seizure burdens associated with ischemia which usually are associated with high morbidity and mortality in cases of HIE in humans (Glass et al., 2009; Jehi et al., 2015) but also led to long-term benefits in alleviating biomarkers of sleep dysfunction and activity-dependent markers of cognition. This rescue was specific to the age P7 vs. P10 and the PB-refractoriness vs. responsiveness of the acute ischemic-seizures, as ANA12 failed to improve or worsened some of long-term outcomes in the P10 group.

Supplementary Material

Refer to Web version on PubMed Central for supplementary material.

Acknowledgement

We thank Brandon Carter and Sunny Thodupunuri for their technical support during this study.

Funding

Research reported in this publication was supported by the Eunice Kennedy Shriver National Institute of Child Health & Human Development of the National Institutes of Health under Award Number R01HD090884 (SDK). The content is solely the responsibility of the authors and does not necessarily represent the official views of the National Institutes of Health.

Abbreviations:

PB	phenobarbital
HIE	hypoxic ischemic encephalopathy
EEG	electroencephalogram
EMG	electromyogram
SWS	slow-wave sleep
P7/P10	postnatal day 7/10

Reference list

Abend NS, and Wusthoff CJ (2012). Neonatal seizures and status epilepticus. J Clin Neurophysiol 29, 441–448. [PubMed: 23027101]

Ahearne CE, Boylan GB, and Murray DM (2016). Short and long term prognosis in perinatal asphyxia: An update. World J Clin Pediatr 5, 67–74. [PubMed: 26862504]

Ajayi OA, Oyaniyi OT, and Chike-Obi UD (1998). Adverse effects of early phenobarbital administration in term newborns with perinatal asphyxia. Trop Med Int Health 3, 592–595. [PubMed: 9705195]

An KM, Ikeda T, Yoshimura Y, Hasegawa C, Saito DN, Kumazaki H, Hirosawa T, Minabe Y, and Kikuchi M (2018). Altered Gamma Oscillations during Motor Control in Children with Autism Spectrum Disorder. J Neurosci 38, 7878–7886. [PubMed: 30104338]

Bales KR, Tzavara ET, Wu S, Wade MR, Bymaster FP, Paul SM, and Nomikos GG (2006). Cholinergic dysfunction in a mouse model of Alzheimer disease is reversed by an anti-A beta antibody. J Clin Invest 116, 825–832. [PubMed: 16498501]

Bittigau P, Sifringer M, and Ikonomidou C (2003). Antiepileptic drugs and apoptosis in the developing brain. Ann N Y Acad Sci 993, 103–114; discussion 123–104. [PubMed: 12853301]

Bjorkman ST, Miller SM, Rose SE, Burke C, and Colditz PB (2010). Seizures are associated with brain injury severity in a neonatal model of hypoxia-ischemia. Neuroscience 166, 157–167. [PubMed: 20006975]

Bortone D, and Polleux F (2009). KCC2 expression promotes the termination of cortical interneuron migration in a voltage-sensitive calcium-dependent manner. Neuron 62, 53–71. [PubMed: 19376067]

Boylan GB, Rennie JM, Pressler RM, Wilson G, Morton M, Binnie CD (2002). Phenobarbitone, neonatal seizures, and video-EEG. Arch Dis Child Feta Neonatal 86, F165–170.

Buzsaki G, and Wang XJ (2012). Mechanisms of gamma oscillations. Annu Rev Neurosci 35, 203–225. [PubMed: 22443509]

Camfield CS, Chaplin S, Doyle AB, Shapiro SH, Cummings C, and Camfield PR (1979). Side effects of phenobarbital in toddlers; behavioral and cognitive aspects. J Pediatr 95, 361–365. [PubMed: 381616]

Cantero JL, Atienza M, Madsen JR, and Stickgold R (2004). Gamma EEG dynamics in neocortex and hippocampus during human wakefulness and sleep. Neuroimage 22, 1271–1280. [PubMed: 15219599]

Carter BM, Sullivan BJ, Landers JR, and Kadam SD (2018). Dose-dependent reversal of KCC2 hypofunction and phenobarbital-resistant neonatal seizures by ANA12. Sci Rep 8, 11987. [PubMed: 30097625]

Chapman KE, Raol YH, and Brooks-Kayal A (2012). Neonatal seizures: controversies and challenges in translating new therapies from the lab to the isolette. Eur J Neurosci 35, 1857–1865. [PubMed: 22708596]

Claassen J, Velazquez A, Meyers E, Witsch J, Falo MC, Park S, Agarwal S, Michael Schmidt J, Schiff ND, Sitt JD, et al. (2016). Bedside quantitative electroencephalography improves assessment of consciousness in comatose subarachnoid hemorrhage patients. Ann Neurol 80, 541–553. [PubMed: 27472071]

Conway JM, Walsh BH, Boylan GB, and Murray DM (2018). Mild hypoxic ischaemic encephalopathy and long term neurodevelopmental outcome - A systematic review. Early Hum Dev 120, 80–87. [PubMed: 29496329]

Dean JC, Hailey H, Moore SJ, Lloyd DJ, Turnpenny PD, and Little J (2002). Long term health and neurodevelopment in children exposed to antiepileptic drugs before birth. J Med Genet 39, 251–259. [PubMed: 11950853]

Donn SM, Grasela TH, and Goldstein GW (1985). Safety of a higher loading dose of phenobarbital in the term newborn. Pediatrics 75, 1061–1064. [PubMed: 4000780]

Farwell JR, Lee YJ, Hirtz DG, Sulzbacher SI, Ellenberg JH, and Nelson KB (1990). Phenobarbital for febrile seizures--effects on intelligence and on seizure recurrence. N Engl J Med 322, 364–369. [PubMed: 2242106]

Gedzelman ER, and Meador KJ (2012). Neurological and psychiatric sequelae of developmental exposure to antiepileptic drugs. Front Neurol 3, 182. [PubMed: 23293628]

Glass HC, Bonifacio SL, Peloquin S, Shimotake T, Sehring S, Sun Y, Sullivan J, Rogers E, Barkovich AJ, Rowitch D, et al. (2010). Neurocritical care for neonates. Neurocrit Care 12, 421–429. [PubMed: 20066514]

Glass HC, Ferriero DM, and Miller SP (2011). Correspondence on “clinical seizures in neonatal hypoxic-ischemic encephalopathy have no independent impact on neurodevelopmental outcome: secondary analyses of data from the neonatal research network hypothermia trial”. J Child Neurol 26, 532; author reply 533–534. [PubMed: 21493809]

Glass HC, Glidden D, Jeremy RJ, Barkovich AJ, Ferriero DM, and Miller SP (2009). Clinical Neonatal Seizures are Independently Associated with Outcome in Infants at Risk for Hypoxic-Ischemic Brain Injury. J Pediatr 155, 318–323. [PubMed: 19540512]

Glass HC, Soul JS, Chu CJ, Massey SL, Wusthoff CJ, Chang T, Cilio MR, Bonifacio SL, Abend NS, Thomas C, et al. (2019). Response to antiseizure medications in neonates with acute symptomatic seizures. Epilepsia.

Gross DW, and Gotman J (1999). Correlation of high-frequency oscillations with the sleep-wake cycle and cognitive activity in humans. Neuroscience 94, 1005–1018. [PubMed: 10625043]

Heinrich H, Busch K, Studer P, Erbe K, Moll GH, and Kratz O (2014). EEG spectral analysis of attention in ADHD: implications for neurofeedback training? Front Hum Neurosci 8, 611. [PubMed: 25191248]

Hellstrom-Westas L, Boylan G, and Agren J (2015). Systematic review of neonatal seizure management strategies provides guidance on anti-epileptic treatment. Acta Paediatr 104, 123–129. [PubMed: 25251733]

Hwang E, McNally JM, and Choi JH (2013). Reduction in cortical gamma synchrony during depolarized state of slow wave activity in mice. Front Syst Neurosci 7, 107. [PubMed: 24379760]

Jehi L, Wyllie E, and Devinsky O (2015). Epileptic encephalopathies: Optimizing seizure control and developmental outcome. Epilepsia 56, 1486–1489. [PubMed: 26293588]

Jiang M, Lee CL, Smith KL, and Swann JW (1998). Spine loss and other persistent alterations of hippocampal pyramidal cell dendrites in a model of early-onset epilepsy. J Neurosci 18, 8356–8368. [PubMed: 9763479]

Jobe AH (2009). Do neonatal seizures cause brain injury? J Pediatr 155, A1.

Johnston MV, Ammanuel S, O'Driscoll C, Wozniak A, Naidu S, and Kadam SD (2014). Twenty-four hour quantitative-EEG and in-vivo glutamate biosensor detects activity and circadian rhythm dependent biomarkers of pathogenesis in Mecp2 null mice. Front Syst Neurosci 8, 118. [PubMed: 25018705]

Kadam SD, and Dudek FE (2007). Neuropathogical features of a rat model for perinatal hypoxic-ischemic encephalopathy with associated epilepsy. J Comp Neurol 505, 716–737. [PubMed: 17948865]

Kadam SD, and Dudek FE (2016). Temporal progression of evoked field potentials in neocortical slices after unilateral hypoxia-ischemia in perinatal rats: Correlation with cortical epileptogenesis. Neuroscience 316, 232–248. [PubMed: 26724579]

Kadam SD, Smith-Hicks CL, Smith DR, Worley PF, and Comi AM (2010a). Functional integration of new neurons into hippocampal networks and poststroke comorbidities following neonatal stroke in mice. Epilepsy Behav 18, 344–357. [PubMed: 20708575]

Kadam SD, White AM, Staley KJ, and Dudek FE (2010b). Continuous electroencephalographic monitoring with radio-telemetry in a rat model of perinatal hypoxia-ischemia reveals progressive post-stroke epilepsy. J Neurosci 30, 404–415. [PubMed: 20053921]

Kang SK, Ammanuel S, Thodupunuri S, Adler DA, Johnston MV, and Kadam SD (2018). Sleep dysfunction following neonatal ischemic seizures are differential by neonatal age of insult as determined by qEEG in a mouse model. Neurobiol Dis 116, 1–12. [PubMed: 29684437]

Kang SK, Johnston MV, and Kadam SD (2015a). Acute TrkB inhibition rescues phenobarbital-resistant seizures in a mouse model of neonatal ischemia. Eur J Neurosci 42, 2792–2804. [PubMed: 26452067]

Kang SK, and Kadam SD (2015). Neonatal Seizures: Impact on Neurodevelopmental Outcomes. Front Pediatr 3, 101. [PubMed: 26636052]

Kang SK, Kim ST, Johnston MV, and Kadam SD (2014). Temporal- and Location-Specific Alterations of the GABA Recycling System in Mecp2 KO Mouse Brains. J Cent Nerv Syst Dis 6, 21–28. [PubMed: 24737935]

Kang SK, Markowitz GJ, Kim ST, Johnston MV, and Kadam SD (2015b). Age- and sex-dependent susceptibility to phenobarbital-resistant neonatal seizures: role of chloride co-transporters. Front Cell Neurosci 9, 173. [PubMed: 26029047]

Kent BA, Michalik M, Marchant EG, Yau KW, Feldman HH, Mistlberger RE, and Nygaard HB (2019). Delayed daily activity and reduced NREM slow-wave power in the APPswe/PS1dE9 mouse model of Alzheimer's disease. Neurobiol Aging 78, 74–86. [PubMed: 30884411]

Kharoshankaya L, Stevenson NJ, Livingstone V, Murray DM, Murphy BP, Ahearne CE, and Boylan GB (2016). Seizure burden and neurodevelopmental outcome in neonates with hypoxic-ischemic encephalopathy. Dev Med Child Neurol 58, 1242–1248. [PubMed: 27595841]

Kim JS, Kondratyev A, Tomita Y, and Gale K (2007). Neurodevelopmental impact of antiepileptic drugs and seizures in the immature brain. Epilepsia 48 Suppl 5, 19–26.

Kwon JM, Guillet R, Shankaran S, Laptook AR, McDonald SA, Ehrenkranz RA, Tyson JE, O'Shea TM, Goldberg RN, Donovan EF, et al. (2011). Clinical seizures in neonatal hypoxicischemic encephalopathy have no independent impact on neurodevelopmental outcome: secondary analyses of data from the neonatal research network hypothermia trial. J Child Neurol 26, 322–328. [PubMed: 20921569]

Lynch M, Sayin U, Bownds J, Janumpalli S, and Sutula T (2000). Long-term consequences of early postnatal seizures on hippocampal learning and plasticity. Eur J Neurosci 12, 2252–2264. [PubMed: 10947804]

Maloney KJ, Cape EG, Gotman J, and Jones BE (1997). High-frequency gamma electroencephalogram activity in association with sleep-wake states and spontaneous behaviors in the rat. Neuroscience 76, 541–555. [PubMed: 9015337]

Markowitz GJ, Kadam SD, Smith DR, Johnston MV, and Comi AM (2011). Different effects of high- and low-dose phenobarbital on post-stroke seizure suppression and recovery in immature CD1 mice. Epilepsy Res 94, 138–148. [PubMed: 21481568]

Mayer SA, Claassen J, Lokin J, Mendelsohn F, Dennis LJ, and Fitzsimmons BF (2002). Refractory status epilepticus: frequency, risk factors, and impact on outcome. Arch Neurol 59, 205–210. [PubMed: 11843690]

McCabe BK, Silveira DC, Cilio MR, Cha BH, Liu X, Sogawa Y, and Holmes GL (2001). Reduced neurogenesis after neonatal seizures. J Neurosci 21, 2094–2103. [PubMed: 11245693]

Mulkey SB, and Swearingen CJ (2014). Advancing neurologic care in the neonatal intensive care unit with a neonatal neurologist. J Child Neurol 29, 31–35. [PubMed: 23271754]

Murray DM, O'Connor CM, Ryan CA, Korotchikova I, and Boylan GB (2016). Early EEG Grade and Outcome at 5 Years After Mild Neonatal Hypoxic Ischemic Encephalopathy. Pediatrics 138.

Nowak M, Zich C, and Stagg CJ (2018). Motor Cortical Gamma Oscillations: What Have We Learnt and Where Are We Headed? Curr Behav Neurosci Rep 5, 136–142. [PubMed: 29862162]

Osredkar D, Toet MC, van Rooij LG, van Huffelen AC, Groenendaal F, and de Vries LS (2005). Sleep-wake cycling on amplitude-integrated electroencephalography in term newborns with hypoxic-ischemic encephalopathy. Pediatrics 115, 327–332. [PubMed: 15687440]

Painter MJ, Scher MS, Stein AD, Armatti S, Wang Z, Gardiner JC, Paneth N, Minnigh B, and Alvin J (1999). Phenobarbital compared with phenytoin for the treatment of neonatal seizures. N Engl J Med 341, 485–489. [PubMed: 10441604]

Pisani F, and Spagnoli C (2016). Neonatal Seizures: A Review of Outcomes and Outcome Predictors. Neuropediatrics 47, 12–19. [PubMed: 26587762]

Rodriguez-Alvarez N, Jimenez-Mateos EM, Dunleavy M, Waddington JL, Boylan GB, and Henshall DC (2015). Effects of hypoxia-induced neonatal seizures on acute hippocampal injury and later-life seizure susceptibility and anxiety-related behavior in mice. Neurobiol Dis 83, 100–114. [PubMed: 26341542]

Rubenstein JL (2010). Three hypotheses for developmental defects that may underlie some forms of autism spectrum disorder. Curr Opin Neurol 23, 118–123. [PubMed: 20087182]

Sohal VS, Zhang F, Yizhar O, and Deisseroth K (2009). Parvalbumin neurons and gamma rhythms enhance cortical circuit performance. Nature 459, 698–702. [PubMed: 19396159]

Williams AE, Giust JM, Kronenberger WG, and Dunn DW (2016). Epilepsy and attention-deficit hyperactivity disorder: links, risks, and challenges. Neuropsychiatr Dis Treat 12, 287–296. [PubMed: 26929624]

Zanettini C, Scaglione A, Keighron JD, Giancola JB, Lin SC, Newman AH, and Tanda G (2018). Pharmacological classification of centrally acting drugs using EEG in freely moving rats: an old tool to identify new atypical dopamine uptake inhibitors. Neuropharmacology.

Zhuang X, Oosting RS, Jones SR, Gainetdinov RR, Miller GW, Caron MG, and Hen R (2001). Hyperactivity and impaired response habituation in hyperdopaminergic mice. Proc Natl Acad Sci U S A 98, 1982–1987. [PubMed: 11172062]

Highlights

- ANA12 alleviates emergence of long-term hyperactivity in mice with history of neonatal seizures
- Significant reversal of disturbed 24h diurnal and sleep-dependent spectral power modulation by ANA12 at P7
- Activity-dependent gamma oscillations restored by ANA12 intervention at P7

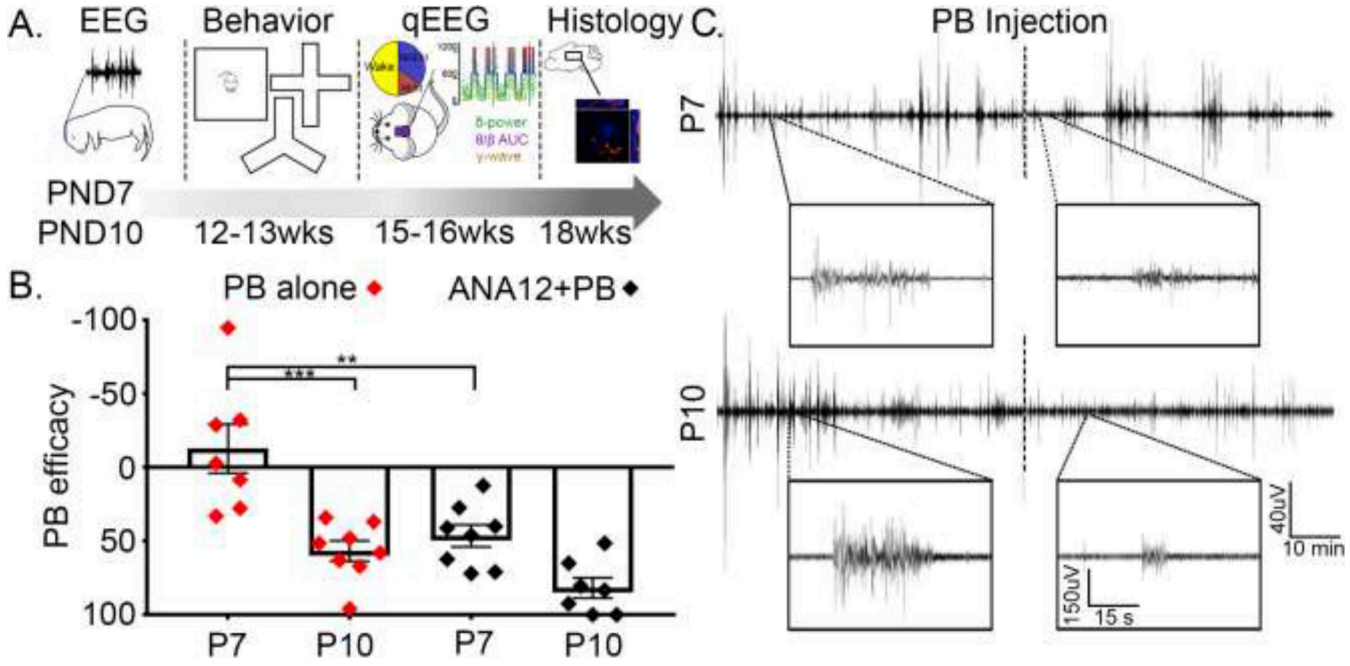

Figure 1. Experimental model.

A. Experimental schematics. **B.** Acute seizure burden profiles, previously shown for the model, were replicated. PB-efficacy was calculated by total seizure burden during post-PB hour divided by total seizure burden during pre-PB hour. PB-efficacy, in the absence of ANA12, was significantly higher in P10 (♦, p=0.0002; One-way ANOVA, $F_{3,26}$=15.15, Bonferroni's multiple comparisons test) compared to P7. ANA12 improved PB-efficacy in P7 (♦ vs. ♦ symbols for P7 groups; p=0.0017). **C.** Representative 1h duration EEG traces of from ANA12+PB group, with magnified 1 min duration traces shown in boxes pre- vs. post-PB; ANA12 was administered prior to the start of recording and time of PB injection is shown with dotted line in the middle. Recording electrodes were placed on the pup's skull overlying the parietal cortex using bregma as a reference. A ground electrode was implanted over the rostrum, and a reference electrode was placed 1cm apart from the recording electrode.

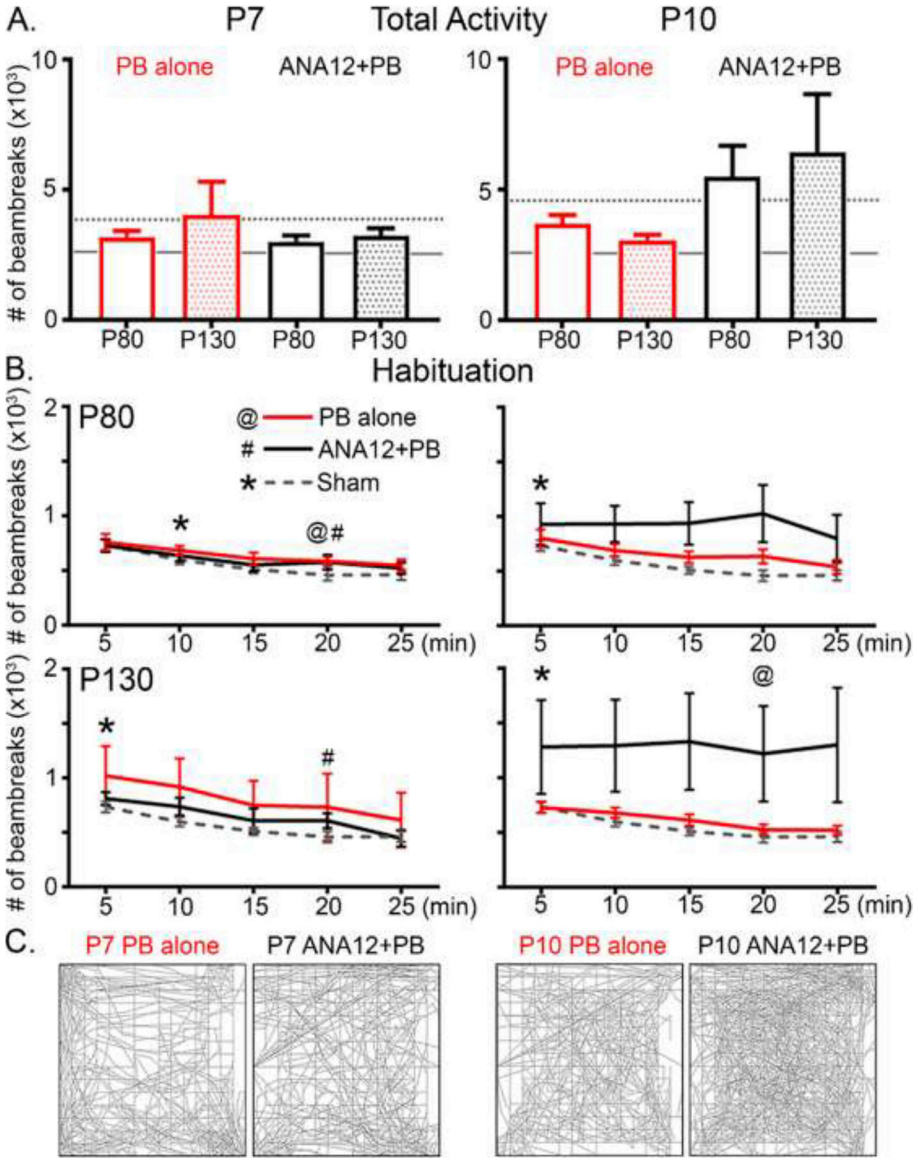

Figure 2. Open field testing.

Open-field testing at P80 and P130 identifies hyperactivity cohort, despite no significant difference in total activity levels measured by the number of beambreaks made by mice during testing. **A.** Total activity levels were not significantly different among groups (p=0.3 $F_{5,49}$=1.25 p=0.4 $F_{5,44}$=0.99 One-way ANOVA; Tukey's, for P80 and P130 in order). P80 and P130 results are shown as clear and shaded bars respectively; age-matched ligate-controls are denoted with dotted line and sham-operated controls in solid line. **B.** Open-field spatial habituation were differential by treatment groups; spatial habituation was determined by α-level (p=0.05) achieved by repeated measures ANOVA compared to the activity level during 1st interval. **C)** Representative traces for each treatment group.

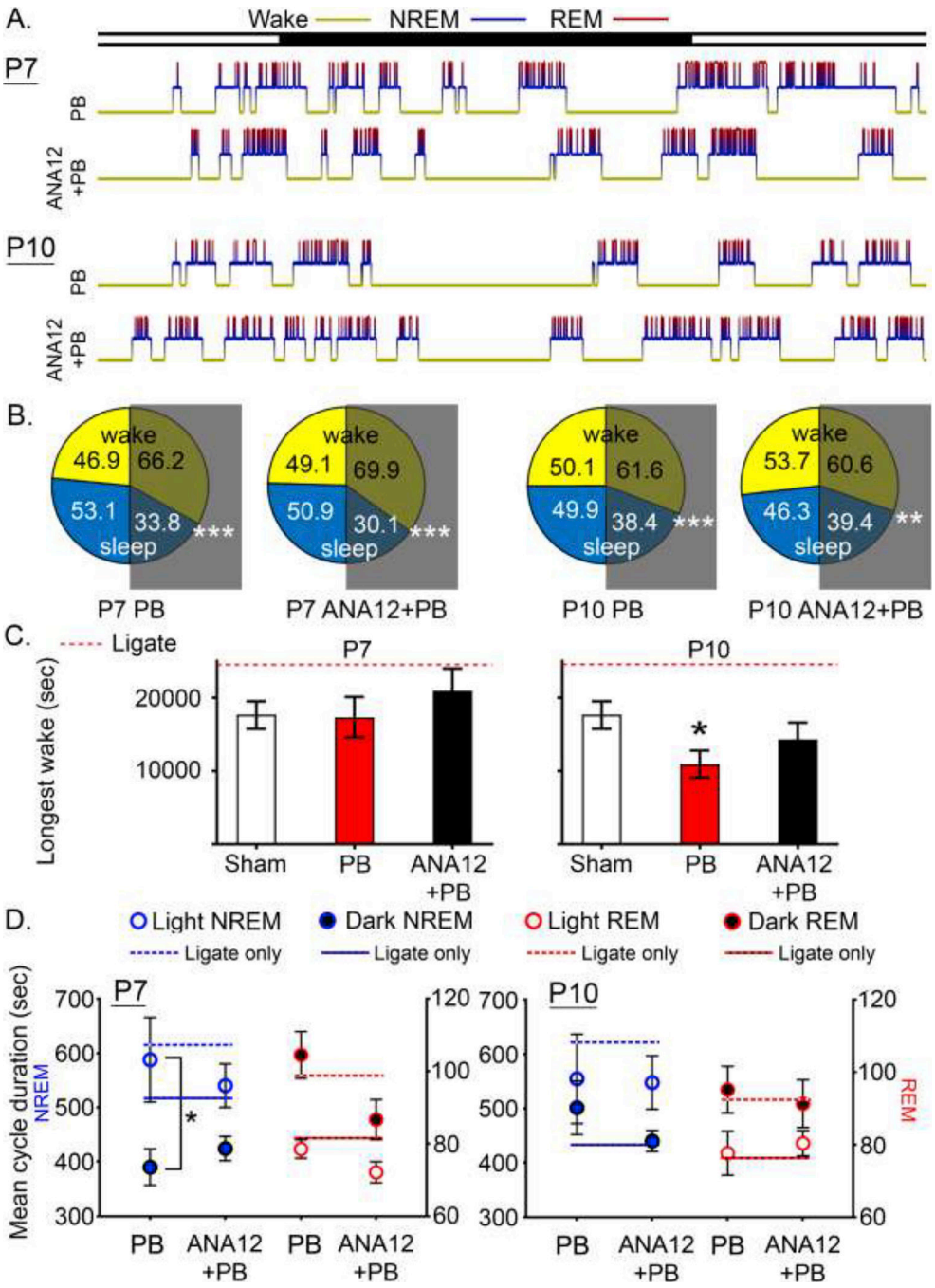

Figure 3. Sleep structure analyses.

A. Representative 24h hypnograms for each treatment group. **B.** Mean percentage of wake and sleep by light and dark cycle. All groups showed significantly higher percent wake vs. sleep ($p<0.01$; white asterisks). **C.** Longest wake cycle for each group. Ligates (untreated and treated ligates) exhibited significantly longer duration of longest wake, and this was reversed in all groups, resulting in loss of statistical significances. P10 PB-alone group had a significantly shorter duration of longest wake compared to sham ($p=0.047$, One-way ANOVA). **D.** Mean cycle duration of NREM and REM by light and dark cycle. Age-

matched untreated ligate-controls are shown in line (dotted for light and solid for dark) for comparison. Asterisk denotes within-group NREM diurnal variation (light vs. dark).

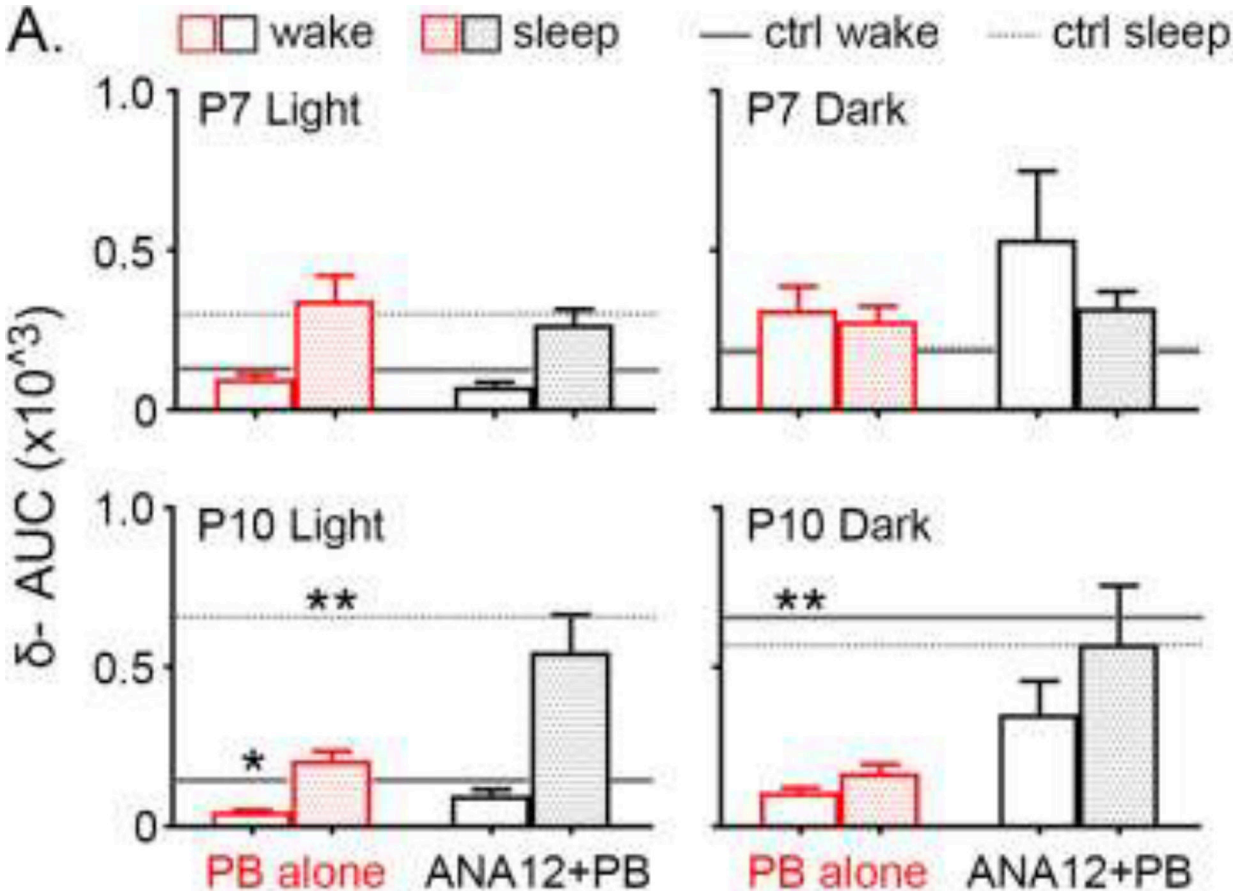

Figure 4. Delta-wave analyses.

Delta-wave AUC were compared to age-matched ligate-controls shown in grey solid (wake) and dotted lines (sleep). Two-way ANOVA analyses confirmed that there is no interaction term between treatment and sleep cycle (p=0.87, 0.63, 0.08, 0.53 from top left to bottom right). P10 PB-alone significantly brought down delta-wave AUC during light cycle for both wake and sleep, and during dark cycle for wake (p=0.0328, p=0.003 and p=0.0011 in order, One-way ANOVA; Tukey's $F_{3,38}$=3.0, 6.6, and 6.3 in order).

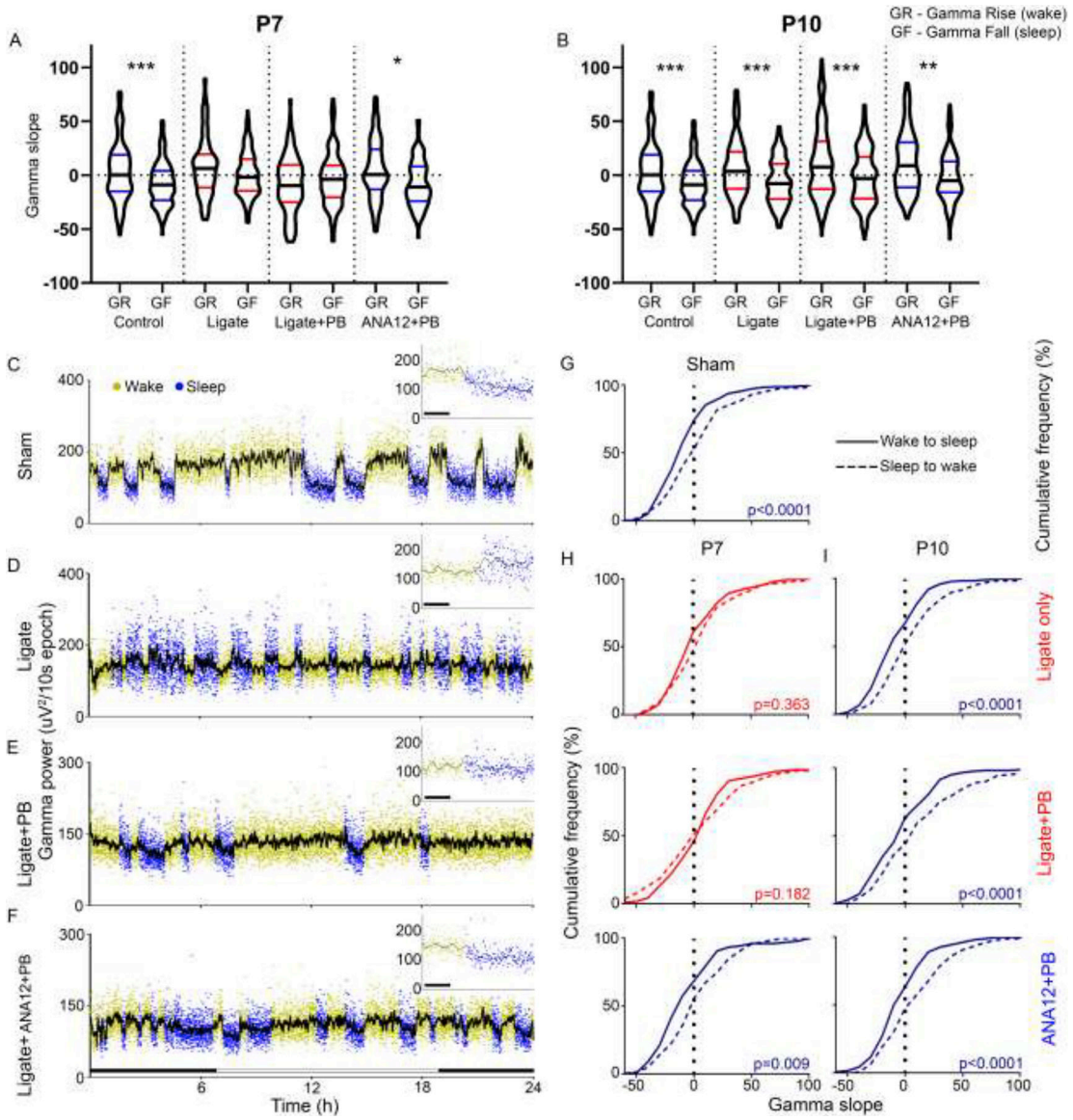

Figure 5. Gamma-wave analyses.

PB significantly alters gamma power during sleep and state-dependent gamma modulation at P7. **A–B.** Gamma slopes were differentially regulated by behavioral-state transitions in the sham-group (Repeated measures ANOVA $F_{7,1293}$=6.76, P<0.0001). The gamma power homeostasis associated with behavioral-state transitions was lost and not statistically significant in the P7 ligate-control and ligate+PB groups (P=0.68, 0.48 respectively). All P10 groups exhibited behavioral state-dependent homeostatic gamma modulation (Repeated measures ANOVA $F_{7,1429}$=13.22). **C–F.** Representative gamma traces over 24h of recording in P7 treatment groups. Red bars indicate detail on top right. **G.** Sham-group gamma slopes are significantly different by behavioral transition (t-test assuming unequal variance; t_{312}<0.0001). P7 ligate-control and ligate+PB lose differential gamma modulation by activity state (Ligate-control: t_{312}=0.363; Ligate+PB: t_{224}=0.182). ANA12+PB rescues state-dependent gamma modulation (t_{222}=0.0086). **I.** At P10, no treatment group loses

resolution between sleep to wake and wake to sleep gamma slope (Ligate: $t_{272}<0.0001$; Ligate+PB: $t_{340}<0.0001$; Ligate+ANA12+PB: $t_{206}=0.0002$).

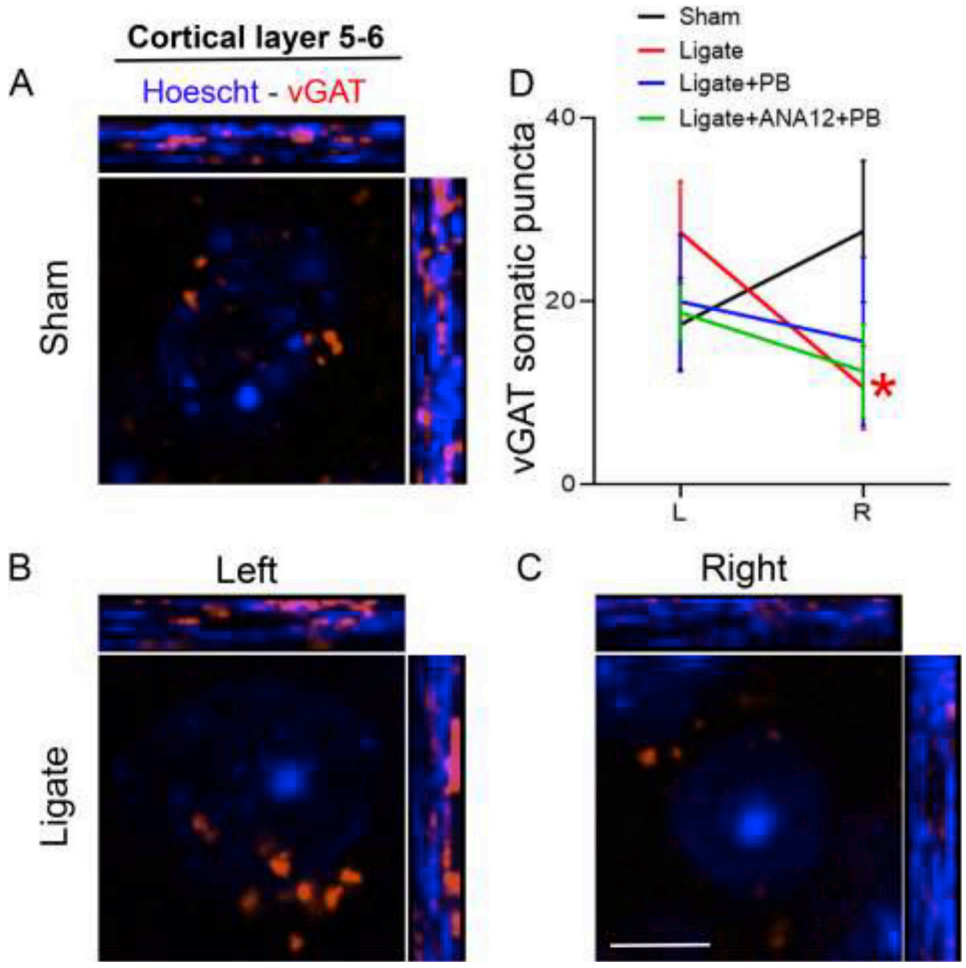

Figure 6.

Immunohistochemical labeling of vGAT followed by quantification of vGAT puncta around perisomatic area in 40x magnification in P7 group. vGAT in red and Hoechst in blue. A. vGAT puncta and nucleus labeling by Hoechst (cortical layer 5–6) in sham brain. B-C. vGAT and Hoechst labeling in brain of ligate-controls show less prominent vGAT puncta around perisomatic area in layer 5–6. D. Pairwise-comparison of somatic vGAT puncta shows a significant reduction in the ipsilateral (right) ischemic side compared to the contralateral (left) for ligate-controls but not for any other groups tested (see Table 4 for details). Scale bar in C = 5um